ICAS 2021 SHANGHAI
International Council of the Aeronautical Sciences
32nd Congress of the International Council of the Aeronautical Sciences
September 6-10, 2021
Pudong Shangri-La, Shanghai, China

TRANSPORT AIRCRAFT WING INVESTIGATIONS AIMED ON WAKE VORTEX IMPACT BY OSCILLATING FLAPS

Johannes Ruhland[1], Florian M. Heckmeier[1] & Christian Breitsamter[1]

[1]Technical University of Munich, Chair of Aerodynamics and Fluid Mechanics, Boltzmannstr. 15, 85748 Garching, Germany

Abstract

The effect of oscillating trailing edge flaps on the wake vortex system of a generic transport aircraft is investigated. The half model presents a high lift configuration (droop nose, advanced dropped hinge flaps) of a generic transport aircraft. For constant temperature anemometry (CTA) measurements, experiments are carried out in the Göttingen-type low-speed wind tunnel C of the Chair of Aerodynamics and Fluid Mechanics of the Technical University of Munich. The experiments are performed at low speed wind tunnel conditions with a Reynolds number of $Re = 0.5 \cdot 10^6$ and a Mach number of $Ma = 0.07$. The wake vortex system of the configuration is captured at cross flow planes perpendicular to the freestream direction at nondimensional distances based on the wing span b of $x/b = (0.064,\ 3,\ 6)$. A baseline configuration with statically deflected flaps is compared to configurations with actuated flaps performing harmonic motions. Both different actuation frequencies $k = (0.04,\ 0.08,\ 0.16)$ and flap amplitudes $\Delta\delta = (2.5°,\ 5°)$ are investigated at $x/b = 6$. It can be shown that a significant disturbance can be imposed already in the extended near field of the wake vortex system for both flap amplitudes, propagating downstream. In addition, all introduced frequencies and higher harmonics are measurable at $x/b = 6$ intended to trigger and enhance the development of wake vortex instabilities fostering wake vortex decay.

Keywords: dynamic flap motion, wake vortex system analysis, constant temperature anemometry

1. Introduction

Efficient aircraft in context of environmental impact and sustainable use of resources are reflected in continuous and intensive research as well as developments improving the aerodynamic performance. Structural and aeroelastic requirements as well as system aspects must be taken into account in order to achieve solutions with high improvement potential. The approach of dynamically moving trailing edge flaps in conjunction with electromechanical actuators makes this possible in an optimal way by combining several aspects. The LuFo V project BIMOD (Influencing maximum lift and wake vortex instabilities by dynamic flap movement), which is conducted by the Institute of Aerospace Systems (RWTH Aachen), the Institute of Structural Mechanics (RWTH Aachen) and the Chair of Aerodynamics and Fluid Mechanics (TU Munich) provides a novel approach combining modern system components to achieve two different effects with one mechanism of action. On the one hand, an increase of the maximum lift is desired and on the other hand, the excitation of wake vortex instabilities to reduce the separation distances between aircraft by means of inversely oscillating flaps is of importance. This paper focuses on influencing the wake vortex system using periodically oscillating flaps. Due to growing difficulties in airport and runway expansion, major airports around the world are facing a long-term capacity problem. The aim is to maintain existing passenger capacities and to reduce the separation distance between two aircraft without reducing the level of safety already obtained today and therewith relieve hub airports. Since in the present work the active influence on the wake vortex system of a transport aircraft is the subject of the investigations, the following short overview of the current state of the art research will only concentrate on such active methods.

Crouch et al. [6] were concerned with the issue of how a periodic movement of the control surfaces

can influence the wake vortex system. For this purpose, numerical simulations as well as experiments in a water tunnel are presented. A four-vortex system was considered, consisting of the wing tip vortex pair and the trailing vortices of the control surfaces located more inboard. Due to the oscillation of the control surfaces, the lift distribution is periodically shifted slightly to outboard and inboard locations. The shifted lift component corresponds to 6% of the total lift. A growth rate of instabilities more than twice as high as for the Crow instability is observed. The experimental investigations in the water tunnel are in agreement with numerical simulations. A significantly earlier formation of vortex rings can be achieved. Transferred to a full-size configuration of a Boeing 747-400, the formation of vortex rings already takes place about 2.5 nautical miles behind the aircraft, whereas without excitation by the control surfaces the vortices would only disintegrate after about 6.5 nautical miles.
Matalanis and Eaton [8] discuss the effect of dynamically deflected Gurney flaps on the characteristics of a wake vortex system consisting of two vortex pairs. This is achieved using a half model featuring a NACA-0012 airfoil. The model has 26 controllable Gurney flaps. With these Gurney flaps disturbances are introduced into the wing tip vortex. Subsequently, the flow pattern in the extended near-field behind the wing is measured and used as input condition for CFD simulations to calculate the development in the far-field of the wake vortex system. The amplitude of perturbations created by the Gurney flaps are on the order of 1% of the vortex spanwise separation and are likely too small to allow pure Crow instability excitation on one vortex pair to occur within a short enough time to effect any reduction of aircraft spacing rules.
Breitsamter and Allen [3] present a more detailed transport aircraft configuration with oscillating winglet-flaps. These flaps can be actuated, whereby the frequency of the oscillation was adjusted to the Crow and Crouch instability. The wake vortex system shows a similar vortex topology for the reference configuration compared to the actuated configuration. However, a spectral analysis of the wake vortex system shows an increase of the amplitudes in the frequency ranges of the Crow and Crouch instability by a factor of 2 to 5. Stimulating the instabilities in the wake by active measures therefore seemed to be within the realm of possibility.
It has already been shown in several publications that an active excitation of instabilities can lead to a faster decay of the wake vortex. However, the majority of the methods presented above referred to largely basic phenomena of multiple vortex systems or required additional systems. Crouch et al. [6] uses the advantage that the flaps are available and no additional high lift system have to be integrated into the wing structure of an aircraft. In this study a half model of a generic transport aircraft configuration with approach settings, equipped with movable trailing edge flaps, is examined. In addition to investigations with static flap deflections, the flaps are also subject to periodic oscillation, which is intended to influence the wake vortex system of the configuration. A time-resolved, phase-locked constant temperature anemometry is used. The wake vortex system between the non-dimensional downstream positions $x/b = (0.064,\ 3,\ 6)$ is investigated, where b denotes the wing span. The reduced frequency k associated with the wavelength λ_{Crow} of the Crow instability [7] is $k_{Crow} \approx (0.056 \pm 0.006) b/b_0$ for $\lambda_{Crow} \approx (9 \pm 1) b_0$ [5]. Here, b_0 is the lateral distance of the rolled up vortices. In addition, the trailing edge flaps are also actuated with lower and higher harmonic frequencies. Two different flap amplitudes $\Delta\delta = (2.5°,\ 5°)$ are examined at $x/b = 6$. The goal is to impose the actuation frequency on the wake vortex structures. This is to be achieved by the actuation frequency of the flaps corresponding to the frequency of the developing instability or higher harmonics.

2. Experimental Setup

2.1 Wind tunnel model

The investigated geometry LR-270 (Long Range 270) is a generic transport aircraft configuration. The half model is subject to the common research program BIMOD (Influencing maximum lift and wake vortex instabilities by dynamic flap movement), which is conducted by the Chair of Aerodynamics and Fluid Mechanics (AER)(Technical University of Munich, TUM), the Institute of Aerospace Systems (RWTH Aachen) and the Institute of Structural Mechanics (RWTH Aachen). Fig. 1 shows an isometric view of the model mounted in the wind tunnel and informations on the geometric parameters are summarized in Tab. 1 [9, 11].

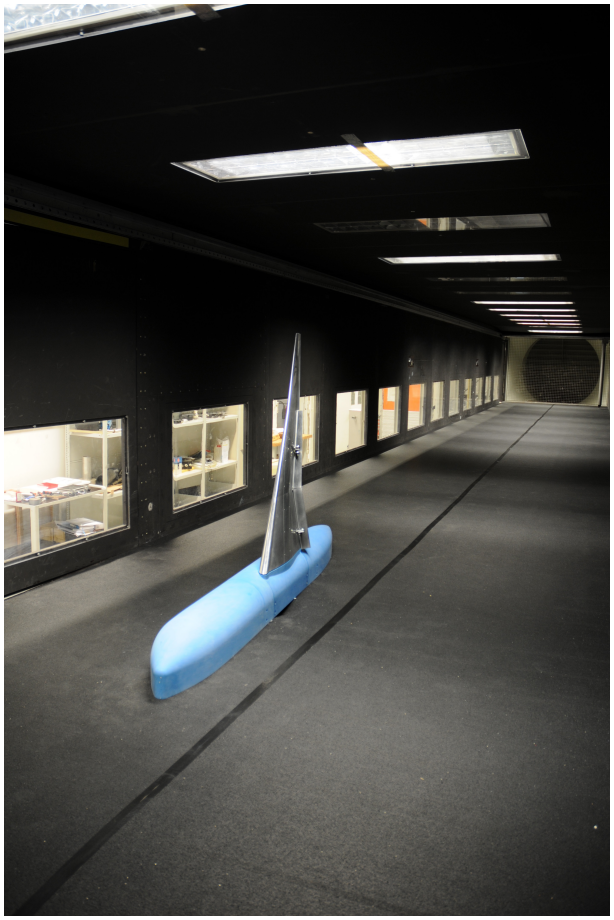

Figure 1 – Wind tunnel model LR-270 mounted in wind tunnel C

To force turbulent boundary-layer characteristics, trip dots are installed at the wing leading edge of the model [4]. The half model presents a high lift configuration (droop nose, advanced dropped hinge flaps) of a generic transport aircraft. The outer flap of the high-lift configuration is divided into two segments, the outboard flap (OF) and the midboard flap (MF). In addition to the possibility of fixed flap deflection angles, there is the opportunity of applying an oscillating motion to the outboard flap and midboard flap with varying frequencies and amplitudes around the chosen flap deflection angle. The inboard flap (IF) is not actuable. To keep the global lift coefficient of the high-lift configuration constant, the outboard and midboard flap oscillate inversely around the adjusted flap deflection angle. The amplitude of the flap movement is determined by an excenter of the driving unit. The frequency of the oscillation can be adjusted via the rotational speed of the motor. Measurements are performed for a configuration without actuated trailing edge flaps (baseline configuration: $k_{act.} = 0$, $\Delta\delta = 0°$) and configurations with actuated trailing edge flaps (actuated configurations: $k_{act.} = (0.04,\ 0.08,\ 0.16)$, $\Delta\delta = (\pm 2.5°,\ \pm 5°)$). The reduced frequency k is defined as:

$$k = \frac{f \cdot (b/2)}{U_{ref}} \tag{1}$$

The wing span is $b = 2.2\ m$ and the freestream velocity amounts $U_{ref} = 25\ m/s$. Fig. 2 shows the outboard and midboard flap motion of the actuated configuration for $\Delta\delta = 5°$. A positive $\Delta\delta$ increases the flap deflection angle and a negative value reduces it. At times $t/T_p = [0,\ 0.5,\ 1.0]$ both flaps have a deflection angle of $25°$. At time $t/T_p = 0.25$, the outboard flap reaches its minimum deflection and the midboard flap its maximum deflection. The deflection of the midboard flap is minimum and the deflection of the outboard flap is maximum at $t/T_p = 0.75$.

Table 1 – Essential geometrical data of the half model LR-270.

Scale			$1:27.7$
Wing			
	Wing half span	$s = b/2$	$1.1\ m$
	Reference area	S_{ref}	$0.233\ m^2$
	Aspect ratio	Λ	8.53
	Taper ratio	λ	0.12
	Reference chord	c_{ref}	$0.312\ m$
	Sweep (25%-line) (inboard/outboard)	φ	$30.08° / 34.25°$
	Dihedral	ν	$\sim 9°$
	Twist	ε	$-1.5°$ to $-4.7°$
	Thickness ratio (in-/mid-/outboard)	c/t	$0.132 / 0.11 / 0.094$
High-Lift Devices			
	Droop nose deflection	DND	$25°$
	Spoiler deflection	SPD	$6.8°$
	Inboard flap deflection	IFD	$20°$ - $40°$ (static)
	Midboard flap deflection	MFD	$20°$ - $40°$ (actuable)
	Outboard flap deflection	OFD	$20°$ - $40°$ (actuable)
Fuselage			
	Length	L	$2.032\ m$
	Diameter	D	$0.220\ m$
	Peniche height	H	$0.075\ m$

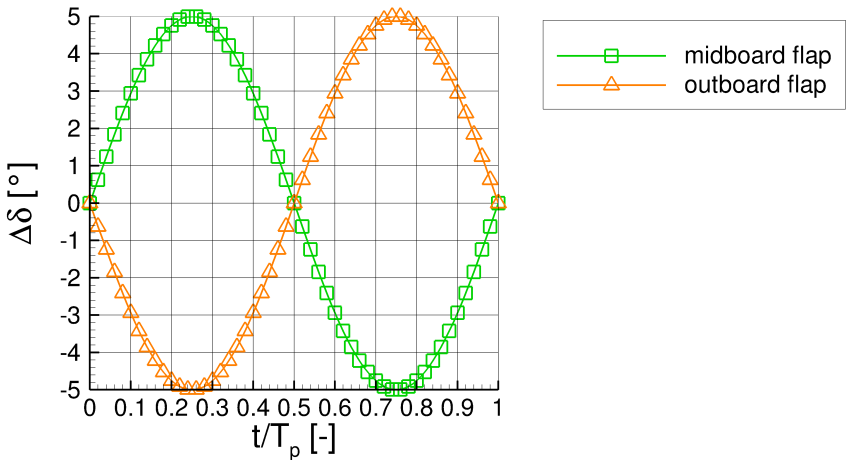

Figure 2 – Midboard and outboard flap motion for actuated configurations, exemplarily shown for the amplitude $\Delta\delta = 5°$

2.2 Test facility

Experiments are carried out in the closed-loop (Göttingen-type) low-speed wind tunnel C (W/T-C) of TUM-AER to conduct triple-wire Constant Temperature Anemometry (CTA) measurements. The W/T-C is operated with a closed test section, which has a size of $1.8 \times 2.7 \times 21\ m^3$ (height x width x length). The ceiling of the wind tunnel is adjustable to minimize the pressure gradient in the longitudinal direction. The turbulence intensity of the freestream is below $Tu < 0.5\%$. The experiments are performed at low subsonic speeds at a Reynolds number of $Re = (U_{ref} \cdot c_{ref})/\nu_{ref} = 0.5 \cdot 10^6$ and a Mach number of $Ma = U_{ref}/a = 0.07$. Here, ν_{ref} denotes the kinematic viscosity and a the speed of sound of the air. As the wing reference point, from which the downstream position of the measured plane is determined, the wing tip trailing edge at an angle of attack of $\alpha = 0.0°$ is chosen. The wake vortex system is captured at cross flow planes perpendicular to the freestream direction at nondimensional distances of $x/b = (0.064,\ 3,\ 6)$ for an angle of attack of $\alpha = 12.0°$ and a lift coefficient of $C_L = 1.4$.

2.3 Measurement setup

Figure 3 shows a schematic sketch of the W/T-C measurement setup. The motor for the flap actuation is controlled by an EPOS program.

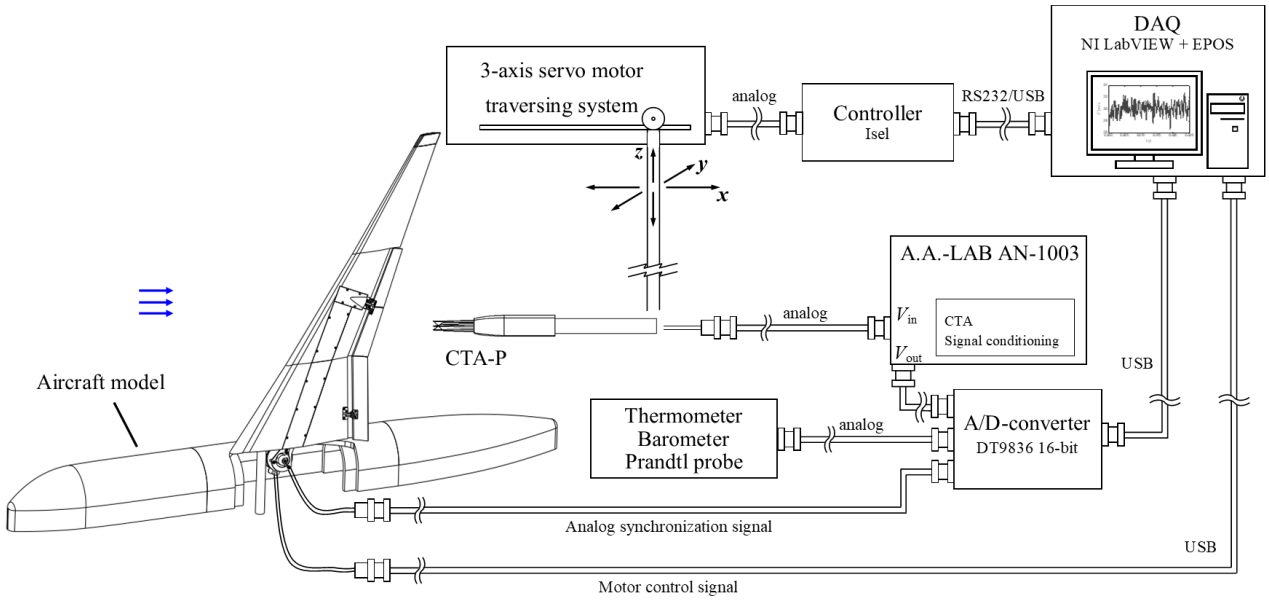

Figure 3 – Hot-wire anemometry and aircraft model measurement setup

Wake measurements of the generic aircraft are conducted with a triple-wire probe (CTA-P), which is mounted on a three-axes traversing system. The servo traversing motors are controlled with an Isel servo-controller that can be automatically controlled within the LabVIEW measurement program. To obtain a time series of axial, lateral, and vertical velocities a triple-wire probe operated by a multichannel CTA system (A.A.-Lab) is used. The hot-wire probe is connected to the A.A.-Lab AN-1003 anemometer [1]. The probe is manufactured in-house at TUM-AER. The wires have a diameter of $5\ \mu m$ and a length of approximately $1.25\ mm$. To achieve the best angular resolution the wires are arranged perpendicular to each other. An additional temperature probe is employed to correct anemometer output voltages if ambient flow temperature varies. Therefore, a linear temperature correction based on Bearman [2] is applied on the measured voltages. A sampling rate of $f_s = 3000\ Hz$, a low pass filter frequency of $f_t = 1000\ Hz$ and a sampling time of $t_s = 6.0\ s$ for the baseline configuration and $t_s = 10.0\ s$ for the actuated configurations are chosen. Considering an exact digital reconstruction of the hot-wire voltage time series, the usable frequency content is limited by the Nyquist frequency, which is half the sampling rate ($1500\ Hz$). Therefore, the analog low pass filter is set to a value lower than the Nyquist frequency to eliminate the frequency content which cannot be captured by the digital reconstruction. The calibration range (velocities $0\ to\ 42\ m/s$ and flow angle $\pm 35°$) are chosen to

capture all values occurring during the flowfield measurements. A look-up table is used to convert the anemometer output signals into the time-dependent axial, lateral, and vertical velocity components u, v, and w. An additional sensor, which is attached to the motor, provides information regarding the current flap positions during a period. This signal is used as a synchronization signal for the time resolved phase-locked measurements for the actuated configurations. Using this signal, the flow field measurements can be assigned to the respective flap positions. Based on statistical error evaluation, accuracies are in the range of 1% for mean quantities, 2.5% for rms quantities (turbulence intensities), and 4% for spectral densities. A more extensive and in-depth discussion of hot-wire measurement technology can be found in [5].

3. Results

The flow field is analyzed for the LR-270 configuration at $\alpha = 12°$, $C_L = 1.4$, $Re = 0.5 \cdot 10^6$ and $Ma = 0.07$ in the cross-flow sections $x/b = [0.064,\ 3,\ 6]$ for the baseline configuration and for the actuated configurations at $x/b = [3,\ 6]$ ($k = (0.04,\ 0.08,\ 0.16)$, $\Delta\delta = (\pm 2.5°,\ \pm 5°)$). The following designations are introduced for the discrete vortices: Wing-tip vortex (WTV), outboard flap vortex (OFV), midboard flap vortex (MFV), inboard flap vortex (IFV) and inboard flap fuselage vortex (IFFV). Individual discrete vortices in turn are formed at the respective side edges of the flaps. For example, the MFV is formed from the discrete vortices, where one forms at the inner side edge of the outboard flap (OF) and the other forms at the outer side edge of the midboard flap (MF). However, these vortices already merge to the MVF in the near field. The same can be seen for the IFV. In the following, the baseline case is investigated first. After that, the actuated flap configurations are studied. The experimental results are compared and discussed.

3.1 baseline configuration

The dominant discrete vortices of the baseline configuration at the measured cross flow sections $x/b = (0.064,\ 3,\ 6)$ are shown in the contour plots of the non-dimensional axial vorticity $\xi_x = \frac{\omega_x b}{2U_{ref}}$ distribution and turbulence intensity $TU = \sqrt{\frac{1}{3}(Tu_x^2 + Tu_y^2 + Tu_z^2)}$ (see fig. 4). As the analysis of the wake vortex flow field focuses on the wing port side the axial vorticity levels are associated with a negative sign for the wing producing lift. The flow field at $x/b = 0.064$ is characterized by five dominant vortices. The WTV, which originates at the wing tip of the configuration, has a vorticity of $\xi_x = -95$. Due to the missing wing tip elements, such as winglet or sharklet, it is strongly dominating. Another highly dominant vortex is the OFV. Its high vorticity ($\xi_x = -38$) is due to the highly loaded OF. Less strongly pronounced vortices are the MFV ($\xi_x = -8$) and the IFV ($\xi_x = -11$), which arise due to the gaps between the associated flaps. The only counterclockwise vortex is the IFFV, which arises due to the interaction between the IF and the fuselage. At $x/b = 0.064$, the IFFV could not be measured because a minimum distance to the fuselage must be maintained with the probe. At the fuselage region, a large zone of increased turbulence intensity is created as a result of the turbulent boundary layers encountered by the wing and fuselage. Due to the turbulent wing boundary layer and the differently directed velocities during the merging of the flow from the upper side of the wing and the lower side of the wing, a shear layer is formed which connects the discrete vortices. This shear layer is reflected as a structured field of increased turbulence intensity clearly separated from the surrounding flow field. The turbulence levels of the shear layer at $x/b = 0.064$ show values of $TU_{max} = 13\%$ for the total turbulence level. The turbulence levels of the free shear layer are significantly increased compared to the free inflow. The vortex centers indicated by the axial vortex strength peak levels corresponds approximately to the turbulence maxima. The further course of the wake vortex system is characterized by the roll-up process or the merging of the discrete vortices and vortex layers. It can be detected that the WTV migrates clockwise around the OFV, which is localized near the center of free circulation [5]. The MFV is merged with the IFV at $x/b = 3$ and also migrates clockwise around the OFV. The IFFV is assignable at $x/b = 3$ in the region ($y/s \approx -0.2,\ z/s \approx -0.55$) via the increased turbulence level. The discrete vortices have lost vorticity. The roll-up process of the wake vortex system can also be followed in the extended near-field by means of the band of locally increased turbulence intensity. Local turbulence maxima are measured in the vortex cores (WTV, OFV, MFV). At $x/b = 6$, the WTV has migrated clockwise almost $270°$ around the OFV. The MFV/IFV also continues

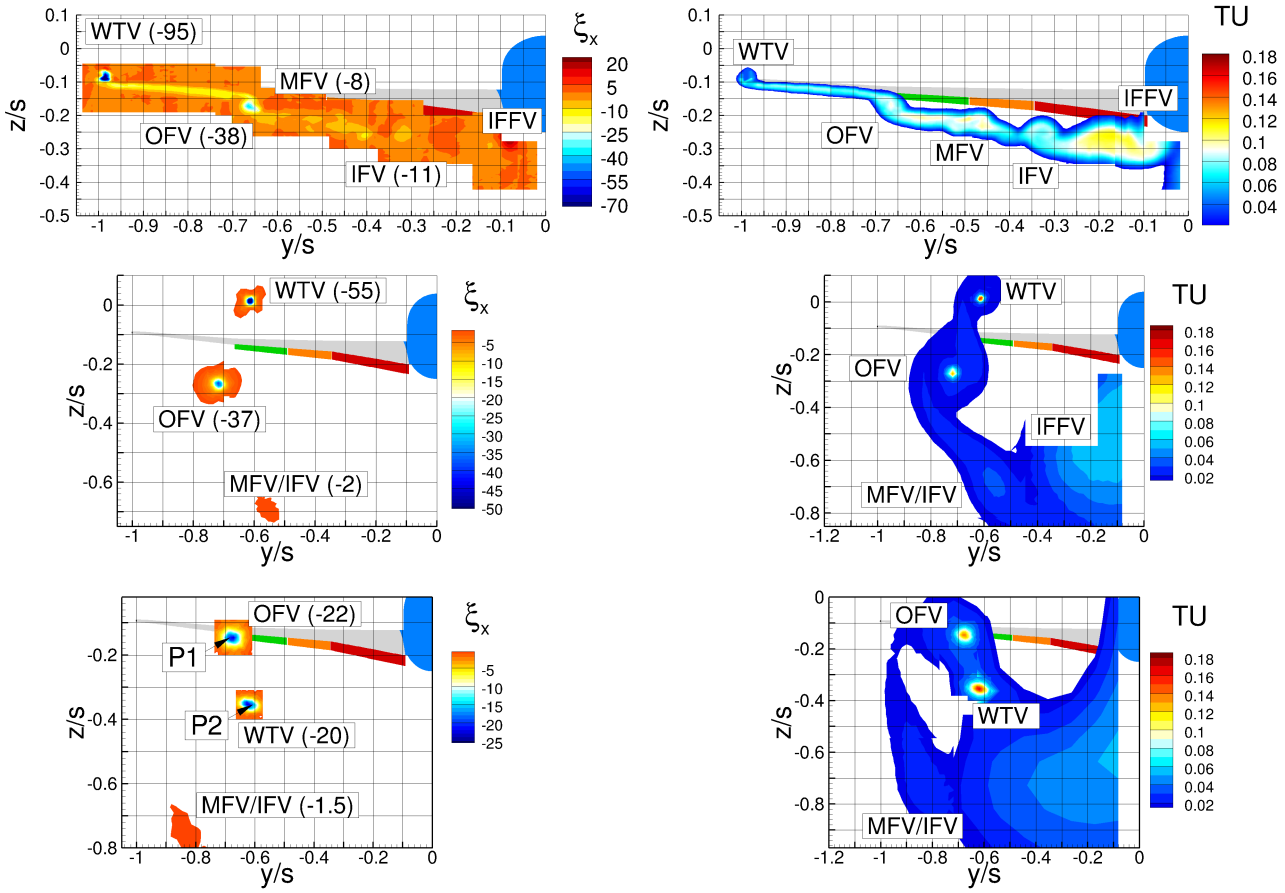

Figure 4 – Contour plots of the non-dimensional axial vorticity and turbulence intensity for the configuration $DND = 25°$, $SPD = 6.8°$, $IFD = MFD = OFD = 25°$, $C_L = 1.4$, $\alpha = 12°$, $Re = 500000$, $Ma = 0.07$, $k_{act.} = 0.00$ and $\Delta\delta = 0°$ at $x/b = (0.064\ (top),\ 3\ (middle),\ 6\ (bottom))$

to roll up around the OFV. The vorticity of the discrete vortices has continued to decrease. The turbulence maxima in the vortex cores of the WTV and OFV have increased up to 17%.

3.2 Actuated configuration

First, the flow field for an actuated configuration ($DND = 25°$, $SPD = 6.8°$, $IFD = MFD = OFD = 25°$, $C_L = 1.4$, $\alpha = 12°$, $Re = 500000$, $Ma = 0.07$) with the parameters $k_{act.} = 0.08$ and $\Delta\delta = 5°$ at the measurement planes $x/b = 3$ and $x/b = 6$ is presented. For the consideration of the near field ($x/b = 0.064$), please refer to [10]. Second, the parameters $k_{act.}$ and $\Delta\delta$ are varied at $x/b = 6$ and the results are compared and discussed.

With respect to the vorticity distribution and the turbulence quantities, a clear difference is found at $x/b = 3$ compared to the baseline configuration (see fig. 5). The vorticity distribution is clearly "smeared" at the positions of the discrete vortices WTV, OFV and MFV and the vorticity centers are not clearly assignable. No striking difference is seen in the IFFV region compared to the baseline configuration. The "smeared" flow field exhibits much lower vorticity peak levels and higher turbulence level maxima.

Also at $x/b = 6$, the behavior of the discrete vortices observed at $x/b = 3$ is confirmed. Fig. 6 shows contour plots of the non-dimensional axial vorticity and turbulence intensity distributions for the configuration $DND = 25°$, $SPD = 6.8°$, $IFD = MFD = OFD = 25°$, $C_L = 1.4$, $\alpha = 12°$, $Re = 500000$, $Ma = 0.07$, $k_{act.} = 0.00$ (top) $k_{act.} = 0.08$ (bottom) and $\Delta\delta = 5°$ at $x/b = 6$. An even wider range of "smeared" vorticity and turbulence distributions can be seen.

This is due to the strong dynamics of the discrete individual vortices (WTV, OFV, MFV, IFV) induced by the oscillating flaps. By linking the measured time series with the respective flap positions, a time-resolved representation of the velocity fields can be used. Fig. 7 shows contour plots of the non-

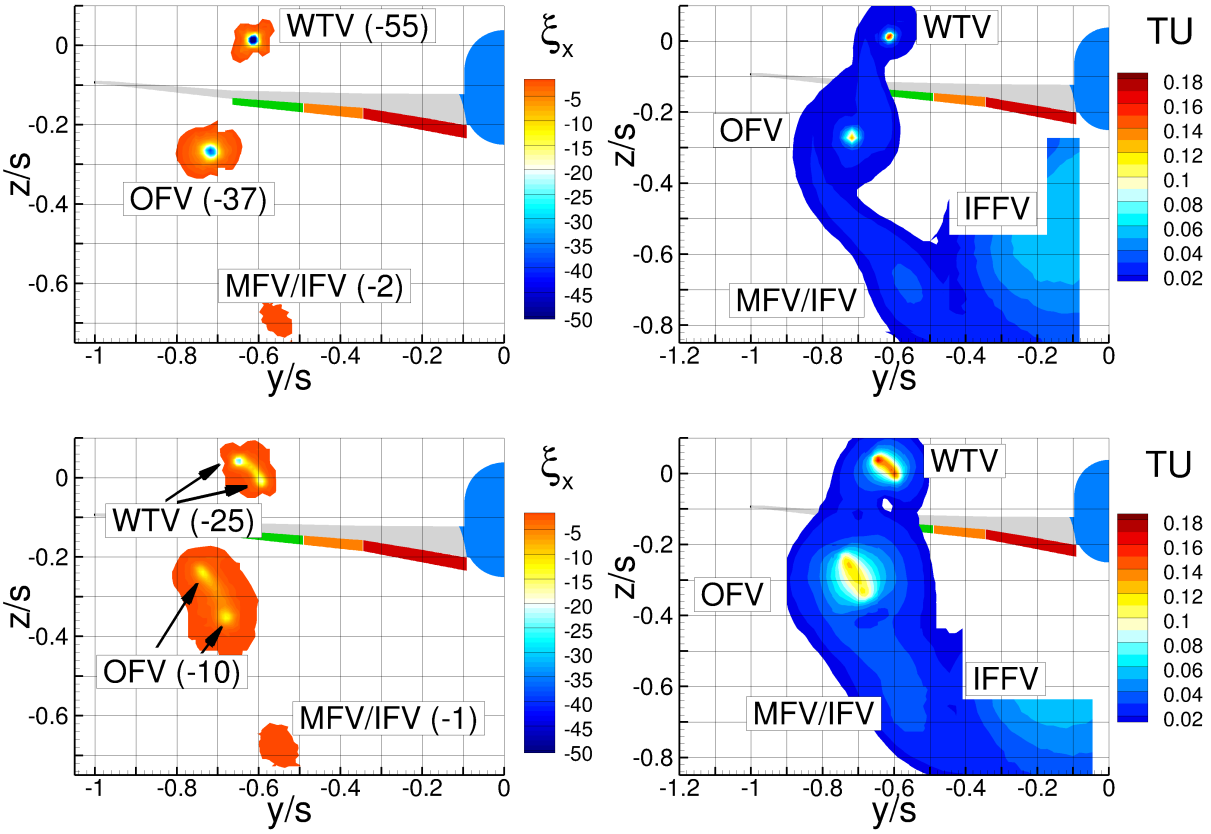

Figure 5 – Contour plots of the non-dimensional axial vorticity and turbulence intensity for the configuration $DND = 25°$, $SPD = 6.8°$, $IFD = MFD = OFD = 25°$, $C_L = 1.4$, $\alpha = 12°$, $Re = 500000$, $Ma = 0.07$, $k_{act.} = 0.00$ (top) $k_{act.} = 0.08$ (bottom) and $\Delta\delta = 5°$ at $x/b = 3$

dimensional axial vorticity and turbulence intensities for the configuration $DND = 25°$, $SPD = 6.8°$, $IFD = MFD = OFD = 25°$, $C_L = 1.4$, $\alpha = 12°$, $Re = 500000$, $Ma = 0.07$, $k_{act.} = 0.08$ and $\Delta\delta = 5°$ at $x/b = 3$ and $t/T_p = (0.00, 0.30, 0.44, 0.68)$. The reason for the strong dynamics of the single vortices is the dynamical merging of the MFV with the IFV or the OFV depending on the flap positions. At time $t/T_p = 0.00$, the MFV disconnects from the IFV and moves towards the OFV to merge with the latter. Due to the change in the vorticity distribution at the entire wake vortex system, the position of the IFV and WTV thus also changes. At time $t/T_p = 0.30$, the MFV and OFV have merged. The position of the vortices reaches one of their maxima of lateral displacements at this time. In the further course of time ($t/T_p = 0.44$) the MFV detaches from the OFV and moves towards the IFV to merge with it. At $t/T_p = 0.68$, the second maximum of lateral displacements of the vortex position is reached. In the following the MFV separates from the IFV and the vortex oscillation starts again.

Also at $x/b = 6$, the behavior of the discrete vortices observed at $x/b = 3$ is confirmed. Fig. 8 shows contour plots of the non-dimensional axial vorticity and turbulence intensity distributions for the configuration $DND = 25°$, $SPD = 6.8°$, $IFD = MFD = OFD = 25°$, $C_L = 1.4$, $\alpha = 12°$, $Re = 500000$, $Ma = 0.07$, $k_{act.} = 0.08$ and $\Delta\delta = 5°$ at $x/b = 6$. The growth of the lateral amplitude $A^* = \sqrt{(\Delta\frac{y}{s})^2 + (\Delta\frac{z}{s})^2}$ of the motion of the discrete vortices with the further downstream development is to be emphasized. The lateral amplitudes A^* of the discrete vortices WTV, OFV, MFV, and IFV are $A^*_{WTV} \approx 0.074$, $A^*_{OFV} \approx 0.127$, $A^*_{MFV} \approx 0.343$, $A^*_{IFV} \approx 0.101$ at $x/b = 3$. In contrast, at $x/b = 6$ the displacements have already increased to: $A^*_{WTV} \approx 0.263$, $A^*_{OFV} \approx 0.222$, $A^*_{MFV} \approx 0.639$. The oscillation of the IFV cannot be determined clearly at $x/b = 6$. The lateral amplitude of the discrete individual vortices increases downstream from $x/b = 3$ to $x/b = 6$.

Now, the parameter $\Delta\delta$ is reduced from $\Delta\delta = 5°$ to $\Delta\delta = 2.5°$. All other configuration settings are retained. Fig. 9 shows contour plots of the non-dimensional axial vorticity and turbulence intensity distributions for the baseline configuration (top) compared to the actuated configurations $DND = 25°$,

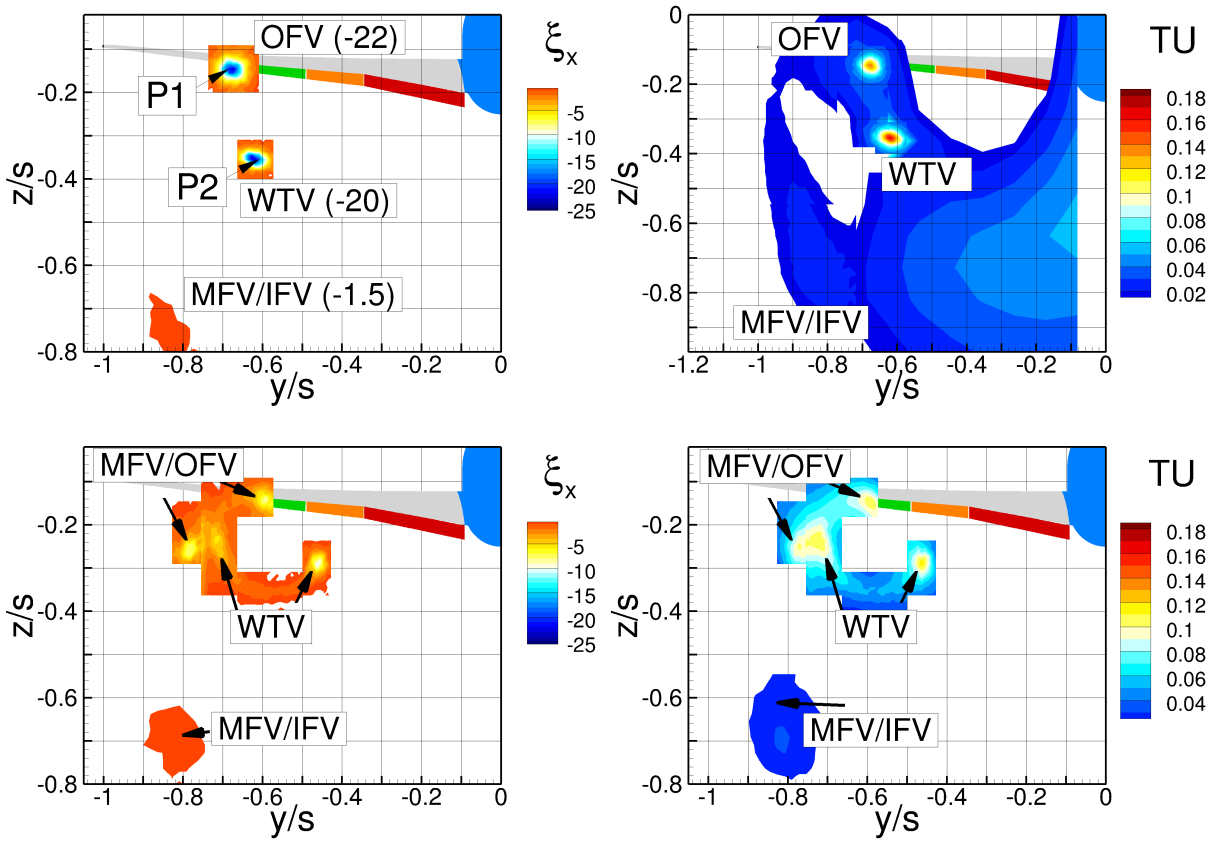

Figure 6 – Contour plots of the non-dimensional axial vorticity and turbulence intensity for the configuration $DND = 25°$, $SPD = 6.8°$, $IFD = MFD = OFD = 25°$, $C_L = 1.4$, $\alpha = 12°$, $Re = 500000$, $Ma = 0.07$, $k_{act.} = 0.00$ (top) $k_{act.} = 0.08$ (bottom) and $\Delta\delta = 5°$ at $x/b = 6$

$SPD = 6.8°$, $IFD = MFD = OFD = 25°$, $C_L = 1.4$, $\alpha = 12°$, $Re = 500000$, $Ma = 0.07$, $k_{act.} = 0.08$ and $\Delta\delta = 5°$ (middle), $\Delta\delta = 2.5°$ (bottom) at $x/b = 6$. Also for the decreased actuation amplitude of the flaps, the phenomenon of dynamic vortex merging observed for the actuation amplitude $\Delta\delta = 5°$ remains. As the actuation amplitude $\Delta\delta$ decreases, the lateral amplitudes A^* of the discrete individual vortices also decrease for $\Delta\delta = 2.5°$: $A^*_{WTV} \approx 0.240$, $A^*_{OFV} \approx 0.198$, $A^*_{MFV} \approx 0.433$ at $x/b = 6$. It should be noted that there is no linear relationship between the actuation amplitude of the trailing edge flaps and the lateral amplitude of the discrete vortices motion.

The actuation frequency of the oscillating flaps is also varied. In addition to the reduced frequencies $k_{act.} = 0.00$ (baseline configuration) and $k_{act.} = 0.08$, the reduced frequencies $k_{act.} = 0.04$ and $k_{act.} = 0.16$ are examined. For this purpose, the points P_1 and P_2 (see fig. 6) are used. Non-dimensional spectral power densities $S^N_{u'}$ of the axial velocity fluctuations u' are evaluated for the points P_1 and P_2 to find peaks in the spectrum associated with the actuation frequency $k_{act.}$. The power densities are plotted in non-dimensional form as a function of the reduced frequency k (see Fig. 10). A direct comparison between the baseline and the actuated configurations is shown. For the actuated configurations, significant peaks can be seen at the associated frequencies for both points. The frequency imposed on the flow field due to the flap oscillations can be detected even after six wing spans.

Thus, it can be assumed that the introduced disturbances due to the oscillating flaps will persist and even increase regarding lateral amplitudes of the vortices downstream, thus resulting in an enhancement of wake vortex decay.

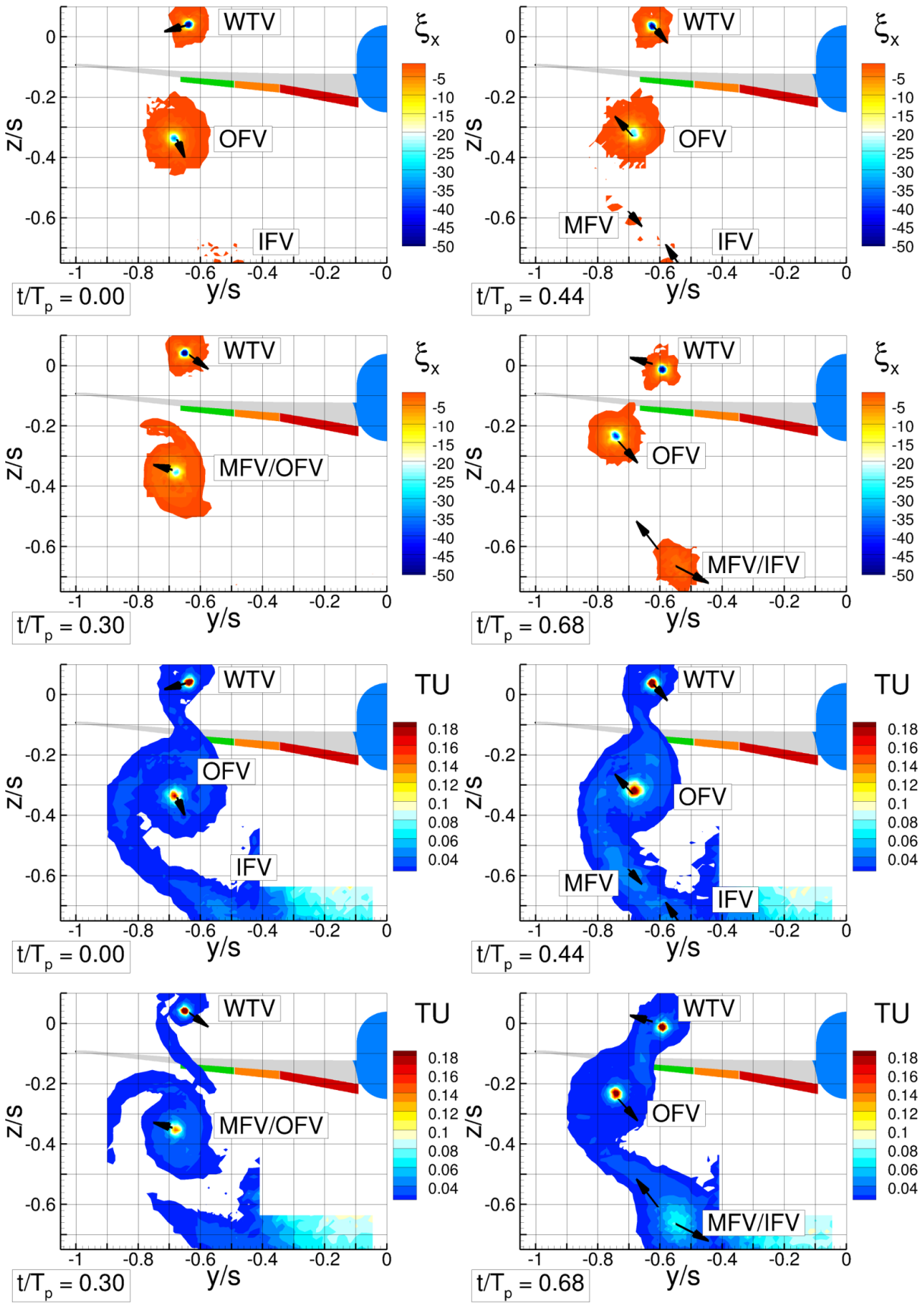

Figure 7 – Contour plots of the non-dimensional axial vorticity and turbulence intensity for the configuration $DND = 25°$, $SPD = 6.8°$, $IFD = MFD = OFD = 25°$, $C_L = 1.4$, $\alpha = 12°$, $Re = 500000$, $Ma = 0.07$, $k_{act.} = 0.08$ and $\Delta\delta = 5°$ at $x/b = 3$ and $t/T_p = (0.00, 0.30, 0.44, 0.68)$

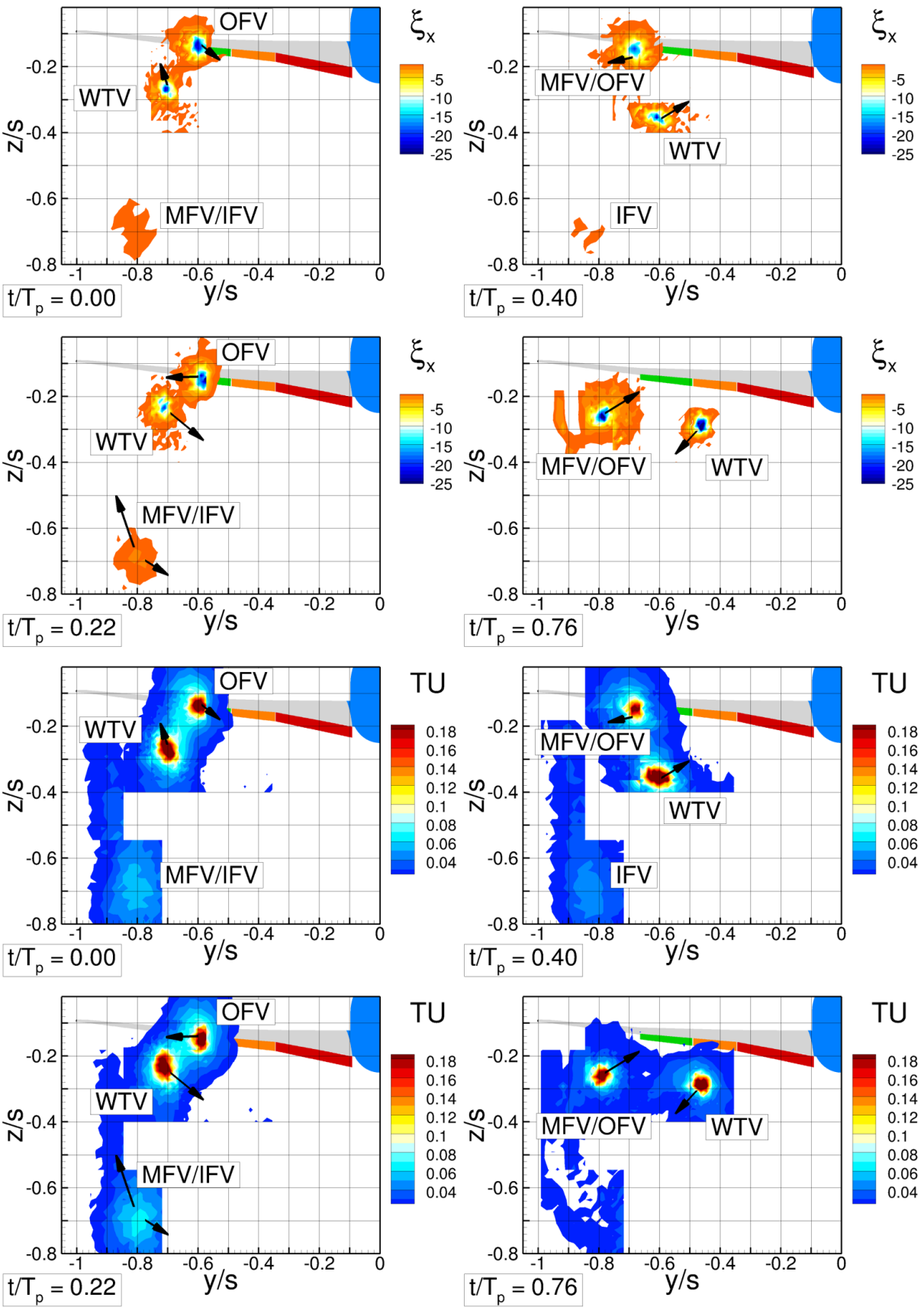

Figure 8 – Contour plots of the non-dimensional axial vorticity and turbulence intensity for the configuration $DND = 25°$, $SPD = 6.8°$, $IFD = MFD = OFD = 25°$, $C_L = 1.4$, $\alpha = 12°$, $Re = 500000$, $Ma = 0.07$, $k_{act.} = 0.08$ and $\Delta\delta = 5°$ at $x/b = 6$ and $t/T_p = (0.00, 0.22, 0.40, 0.76)$

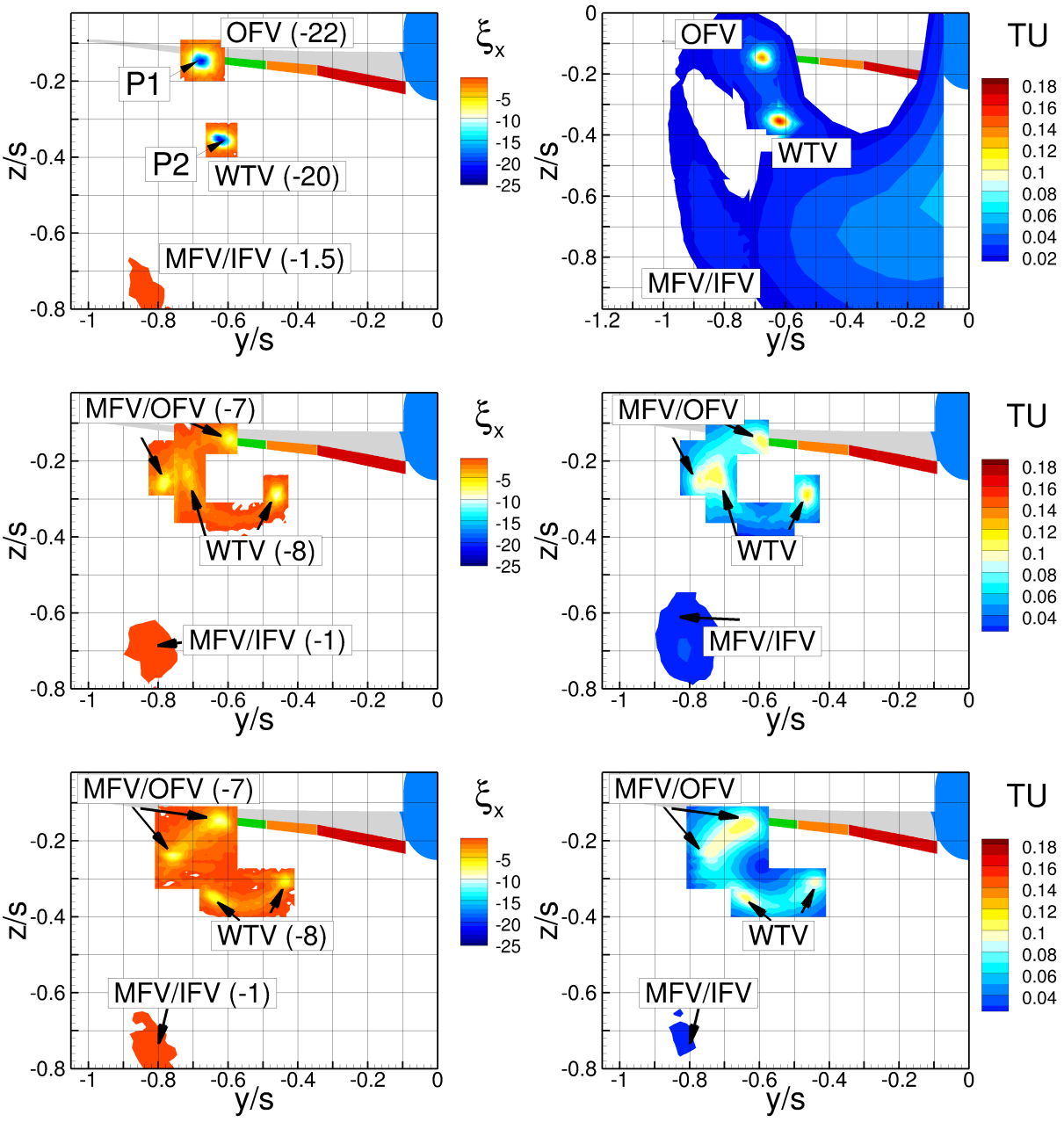

Figure 9 – Contour plots of the non-dimensional axial vorticity and turbulence intensity for the baseline configuration (top) and actuated configurations $DND = 25°$, $SPD = 6.8°$, $IFD = MFD = OFD = 25°$, $C_L = 1.4$, $\alpha = 12°$, $Re = 500000$, $Ma = 0.07$, $k_{act.} = 0.08$ and $\Delta\delta = 5°$ (middle), $\Delta\delta = 2.5°$ (bottom) at $x/b = 6$

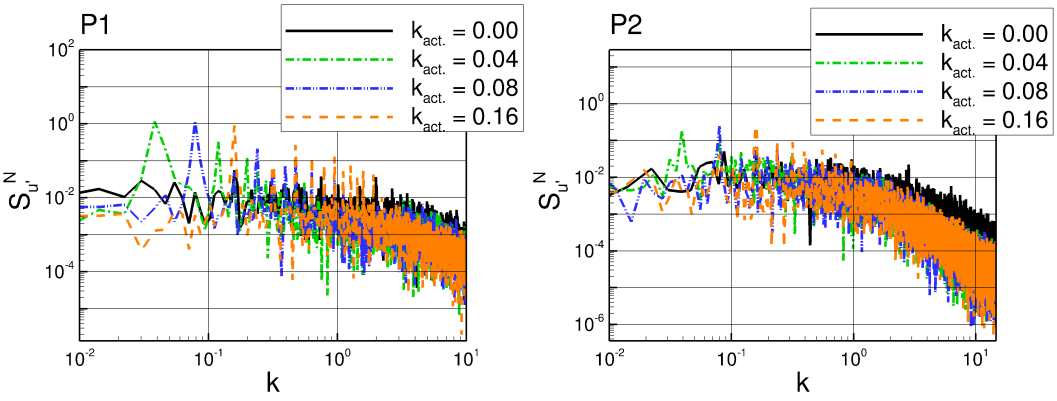

Figure 10 – Spectral power densities $S^N_{u'}$ of the axial velocity fluctuations u' at the points P_1 and P_2 for the configuration $DND = 25°$, $SPD = 6.8°$, $IFD = MFD = OFD = 25°$, $C_L = 1.4$, $\alpha = 12°$, $Re = 500000$, $Ma = 0.07$ and $\Delta\delta = 5°$ at $x/b = 6$ for $k_{act.} = (0.00,\ 0.04,\ 0.08,\ 0.16)$

4. Conclusion

The present investigations concentrate on forced motion disturbances on the wake vortex system of a generic transport aircraft already in the extended near field by means of oscillating flaps. In this way, a long-wave instability (Crow instability) is supposed to be excited in the farther downstream course of the wake vortex system development. The generic transport aircraft model is investigated under wind tunnel conditions at Mach number $Ma = 0.07$ and at a Reynolds number of $Re = 0.5 \cdot 10^6$ with approach high lift settings (angle of attack $\alpha = 12°$, lift coefficient $C_L = 1.4$, flap settings $25°$, droop nose deflection $25°$ and spoiler deflection $6.8°$). A baseline configuration case with static flap deflection is compared to configurations with two oscillating trailing edge flaps with the model featuring an inboard and a spanwise splitted midboard/outboard flap. The inboard flap is at any time statically deflected. The midboard and outboard flaps can be actuated inversely. Triple wire phase-locked synchronized constant temperature anemometry measurements are conducted.
A strong disturbance that is introduced into the flow field by means of oscillating flaps is detected. A highly dynamic vortex movement including vortex merging and non-merging, especially in the farther downstream section at $x/b = 3$ and $x/b = 6$, is observed. The relationship between the actuation amplitude of the flaps with the lateral amplitude of the discrete vortex motion is not linear. Thus, even with a reduced actuation amplitude by half ($\Delta\delta = 2.5°$ instead of $\Delta\delta = 5°$ flap amplitude), significant vortex dynamics and lateral amplitudes can be excited at $x/b = 6$. The actuation frequencies ($k_{act.} = (0.04,\ 0.08,\ 0.16)$) imposed on the flow field due to the flap oscillations can be detected at $x/b = 6$. The further downstream development of the wake vortex system will be modeled and calculated in further work by means of numerical methods.

5. Acknowledgments

The funding of this investigation within the LUFO V3 project BIMOD (FKZ: 20E1702C) by the German Federal Ministry for Economic Affairs and Energy (BMWi), is gratefully acknowledged.

6. Contact Author

mailto: johannes.ruhland@tum.de

7. Copyright statement

References

[1] A.A. Lab Systems. AN-1003 Hot-Wire and Film Anemometry Systems - User's Manual. *A.A. Lab Systems LTD*, 1999.

[2] Bearman P.W. Corrections for the effect of ambient temperature drift on hot-wire measurements in incompressible flow. *DISA Inf.*, 11(11), pp 201–208, 1971.

[3] Breitsamter C and Allen A. Transport Aircraft Wake Influenced by Oscillating Winglet Flaps. *Journal of Aircraft*, Vol. 46, pp 175-188, 2009.

[4] Breitsamter C. Strömungsphysik und Modellgesetze. *Technische Universität München*¶, 2018.

[5] Breitsamter C. Wake vortex characteristics of transport aircraft. *Progress in Aerospace Sciences*, Vol. 47, No. 2, pp. 89-134, 2011.

[6] Crouch J D, Miller G D and Spalart P R. Active-Control System for Breakup of Airplane Trailing Vortices. *AIAA Journal*, Vol. 1, No. 12, pp 2374-2381, 2001.

[7] Crow SC. Stability Theory for a Pair of Trailing Vortices. *AIAA*, Vol. 8(12), pp 2171-2179, 1970.

[8] Matalanis Claude G and Eaton J K. Wake Vortex Alleviation Using Rapidly Actuated Segmented Gurney Flaps. *AIAA Journal*, Vol. 45, No. 8, pp 1874-1884, 2007.

[9] Ruhland J and Breitsamter C. Numerical analysis of high-lift configurations with oscillating flaps. *CEAS Aeronautical Journal*, Vol. 12, pp 345–359, 2021.

[10] Ruhland J and Breitsamter C (in press). Wake Vortex Analysis on Transport Aircraft Wing featuring Dynamic Flap Motion. *Notes on Numerical Fluid Mechanics and Multidisciplinary Design*

[11] Stephan R et al. Influence of dynamic flap movement on maximum lift and wake vortex evolution. *Deutscher Luft- und Raumfahrtkongress*, Darmstadt, 2019.